ACS NANO

www.acsnano.org

ARTICLE

Demonstration of Stochastic Resonance, Population Coding, and Population Voting Using Artificial MoS_2 Based Synapses

Akhil Dodda and Saptarshi Das*

Cite This: *ACS Nano* 2021, 15, 16172–16182

Read Online

ACCESS | Metrics & More | Article Recommendations | Supporting Information

ABSTRACT: Fast detection of weak signals at low energy expenditure is a challenging but inescapable task for the evolutionary success of animals that survive in resource constrained environments. This task is accomplished by the sensory nervous system by exploiting the synergy between three astounding neural phenomena, namely, stochastic resonance (SR), population coding (PC), and population voting (PV). In SR, the constructive role of synaptic noise is exploited for the detection of otherwise invisible signals. In PC, the redundancy in neural population is exploited to reduce the detection latency. Finally, PV ensures unambiguous signal detection even in the presence of excessive noise. Here we adopt a similar strategies and experimentally demonstrate how a population of stochastic artificial neurons based on monolayer MoS_2 field effect transistors (FETs) can use an optimum amount of white Gaussian noise and population voting to detect invisible signals at a frugal energy expenditure (~10s of nano-Joules). Our findings can aid remote sensing in the emerging era of the Internet of things (IoT) that thrive on energy efficiency.

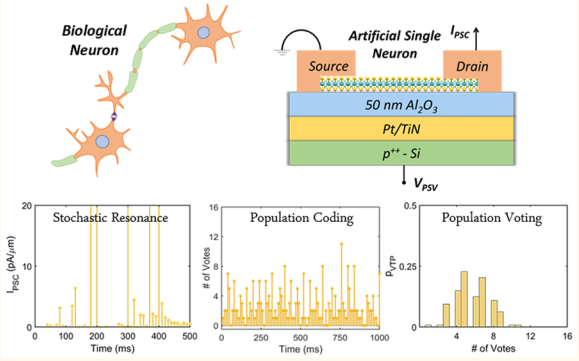

KEYWORDS: *two-dimensional materials, stochastic resonance, population coding, population voting, subthreshold signal detection, low-power sensors, monolayer MoS_2 field effect transistors*

Early detection of weak signals is essential for the survival of many animals, especially those living in resource constrained environments. Both experimental and numerical studies have found that inherent neural noise can play a constructive role in the detection of subthreshold sensory signals, allowing animals to escape from predators or locate prey. This phenomenon is more popularly known as stochastic resonance (SR) and is observed at molecular, cellular and behavioral levels.[1−5] For example, the electroreceptors in paddlefish use SR to detect zooplankton for food,[2] mechanoreceptors in crickets use SR to escape from predatory wasps,[3] and infrared (IR) sensilla in jewel beetles use SR to locate forest fires for breeding.[5] However, reliable and timely detection of subthreshold signals using SR can be severely limited if the nervous system employs individual neurons for such tasks. At low noise levels, the likelihood that the subthreshold sensory signal will cross the neural detection threshold, that is, probability of true positive (TP) remains low, whereas at high noise levels the likelihood of false positive (FP), that is, neurons firing even in the absence of any stimulus, becomes high. Furthermore, the stochastic nature of the signal processing does not guarantee instantaneous detection of the subthreshold sensory signal since threshold crossing will not occur every time the same stimulus is presented.

While SR experiments overcome this challenge by relying on periodic signals to present the subthreshold stimulus multiple times to the neuron and evaluate the detection probability to show the constructive role of noise in signal detection, these experiments do not provide complete understanding of the animal behavior since survival strongly depends on immediate response to weak stimulus. The evolutionary answer for this challenging problem may lie in population coding (PC) and population voting (PV), where instead of relying on a single neuron, the synergistic activity of the neural population is exploited for accurate and immediate detection of subthreshold

Received: June 13, 2021
Accepted: September 29, 2021
Published: October 14, 2021

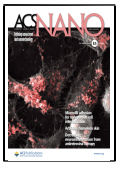

https://doi.org/10.1021/acsnano.1c05042
ACS Nano 2021, 15, 16172–16182

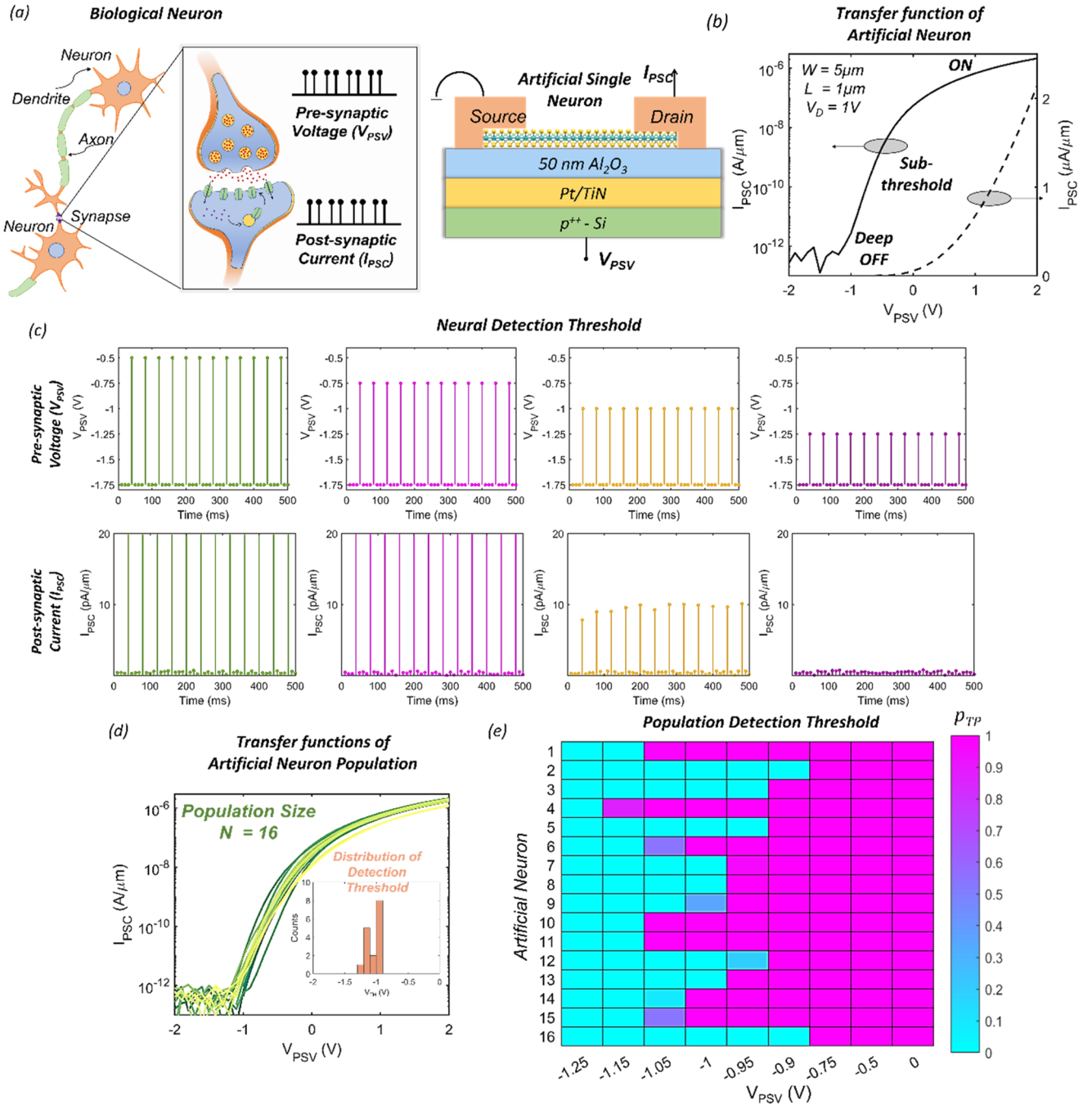

Figure 1. Artificial Neural Population. (a) Schematic of biological neuron and artificial neuron based on monolayer MoS_2 field effect transistor (FET). MoS_2 was grown over large area using metal organic chemical vapor deposition (MOCVD) technique on sapphire substrate at 1000 °C and subsequently, transferred to the device fabrication substrate using the PMMA-assisted wet transfer process. Atomic layer deposition (ALD) grown 50 nm Al_2O_3 on Pt/TiN/p^{++}-Si was used as the back-gate stack for the fabrication of MoS_2 FET. Device has 1 μm channel length, 5 μm channel width, and 40 nm Ni/30 nm Au as the source/drain contacts. Presynaptic voltage (V_{PSV}) is applied to the back-gate terminal, whereas, postsynaptic current (I_{PSC}) is measured at the drain terminal. (b) Transfer function, that is, I_{PSC} versus V_{PSV} of a representative artificial neuron measured at drain bias, V_D = 1 V, in the logarithmic and linear scales. (c) Neural detection threshold: Recording of postsynaptic spikes in I_{PSC} (lower panel) in response to presynaptic V_{PSV} pulses of different magnitudes (upper panel). Postsynaptic firing disappears as the magnitude of V_{PSV} pulses falls below the detection threshold (V_{TH}), which in the present case was found to be V_{TH} = −1.25 V. V_{TH} is determined by the minimum I_{PSC} measurable by the neuron that is above the instrument noise floor of few pico Amperes. This corresponds to the deep OFF state of the MoS_2 FET. (d) Population transfer function of N = 16 artificial neurons. Variation in the transfer function is a key feature of any neural population, which is naturally present in MoS_2 FET array. Inset shows the histogram of the V_{TH} for the neural population with population mean and standard deviation of be −1.05 V and ∼0.1 V, respectively. (e) Colormap of probability of true positive (p_{TP}), that is, the likelihood of a postsynaptic spike when a presynaptic stimulus is present for each neuron in the population as a function of V_{PSV}. In the absence of any noise each neuron behave deterministically, that is, p_{TP} = 1, for suprathreshold signals, and p_{TP} = 0, for subthreshold signal.

https://doi.org/10.1021/acsnano.1c05042
ACS Nano 2021, 15, 16172−16182

sensory inputs.[6−10] Extensive studies on the visual cortex of macaque monkeys,[10] auditory midbrain of guinea pigs,[7] and somatosensory cortex of rats[11] provide direct evidence of PC for suprathreshold signal detection as several thousand of neurons are found to respond to similar stimuli. Evidence of PV was found in motor cortical neurons.[12,13] However, the benefits of PC and PV for subthreshold signal detection is relatively underexplored.[14] Furthermore, the interdependence between neural stochasticity, neural population strength, neural voting mandate, neural detection limit, and subthreshold signal strength is not well understood and is a subject of intense research in modern sensory neurobiology.

Here, we attempt to answer these fundamental questions using an array of nanoscale field effect transistors (FETs) based on atomically thin monolayer MoS_2 that mimics a stochastic neural population. Our experimental findings validated by numerical simulations suggest that in the presence of an optimum amount of white Gaussian noise a sensor population of optimum size can decisively vote to accurately detect otherwise invisible signals with significantly reduced detection latency and miniscule energy expenditure. Our demonstration highlights the benefits of adopting SR, PC, and PV for next generations of remote sensors, which will be deployed at inaccessible, and resource-constrained terrestrial and extraterrestrial locations as a part of the rapidly proliferating Internet of things (IoT) ecosystem. Note that while the concept of SR has been demonstrated using electronic and optoelectronic devices such as tunnel diodes,[15] photodetectors,[16] and field effect transistors (FETs) based on carbon nanotubes,[17,18] GaAs nanowires,[19] and organic semiconductors,[20] the benefits of synergy between SR, PC, and PV is yet to be exploited in solid state sensors.

RESULTS AND DISCUSSION

Fabrication and Characterization of Artificial Neural Population. Monolayer MoS_2 belonging to the family of layered two-dimensional (2D) transition metal dichalcogenides (TMDCs)[21−23] was used as the semiconducting channel material and atomic layer deposition (ALD) grown 50 nm Al_2O_3 on Pt/TiN/p^{++}-Si was used as the back-gate stack for the fabrication of artificial neurons as shown schematically in Figure 1a. Presynaptic signals were applied to the back-gate terminal and, postsynaptic current was measured at the drain terminal. Note that atomically thin 2D semiconductors such as monolayer MoS_2 offer potential for aggressive device scaling and high dielectric constant of Al_2O_3 compared to conventional SiO_2 allows for superior electrostatic gate control, essential for achieving low power device operation.[24] The choice of MoS_2 is motivated by its technological maturity, which include high electrical performance, ease of fabrication, ease of growing over a large area (wafer-scale), high yield, low device-to-device variation, reliability, and demonstration of multifunctional sensors as well as biomimetic, neuromorphic, and hardware security devices.[25−36] MoS_2 used in this study was grown epitaxially on a sapphire substrate using a metal organic chemical vapor deposition (MOCVD) technique at 1000 °C and subsequently transferred from the growth substrate to the device fabrication substrate using a PMMA-assisted wet transfer process.[37] The large-area MOCVD growth allows for the fabrication of high-performance monolayer MoS_2 FET arrays that serve as the neural population. See Methods for further details on the synthesis, film transfer, and fabrication of monolayer MoS_2 FETs.

Figure 1b shows the transfer function, that is, postsynaptic current (I_{PSC}) as a function of presynaptic voltage (V_{PSV}) of a representative artificial neuron measured at a drain bias (V_D) of 1 V, in the logarithmic and linear scales. The *n-type* unipolar characteristics shown is typical for MoS_2 FETs owing to the phenomenon of metal Fermi level pinning close to the conduction band of MoS_2 that facilitates electron injection.[24,38] The transfer function was used to extract at ON/OFF current ratio in excess of 10^7, a subthreshold slope (SS) of less than 300 mV/decade, and a field effect mobility value of ∼10 cm^2/V-s from the peak transconductance. These numbers are comparable to exfoliated single crystal monolayer MoS_2 based FETs indicating high-quality MOCVD growth (see Supporting Information 1 for Raman and PL and AFM measurements). Note that the device has 1 μm channel length, 5 μm channel width, and 40 nm Ni/30 nm Au as the source/drain contacts. Since an MoS_2 FET is a thresholding device, we determine the detection limit of our artificial neuron by applying V_{PSV} pulses of different magnitudes and recording the corresponding spikes in I_{PSC} as shown in Figure 1c. Clearly postsynaptic firing, that is, spikes in $I_{PSC,}$ disappears as the magnitude of the V_{PSV} pulses falls below the detection threshold (V_{TH}) of the neuron, which in the demonstrated case was found to be V_{TH} = −1.25 V. Note that V_{TH} is determined by the minimum I_{PSC} measurable by the neuron that is above the instrument noise floor of a few pico-Amperes. This corresponds to the deep OFF state of the MoS_2 FET, as shown in Figure 1b.

Figure 1d shows the transfer functions of the N = 16 artificial neurons used in this study. Variation in the transfer function is a key feature of any neural population and is naturally present in our large-area MOCVD-grown monolayer MoS_2 FET array. The colormap in Figure 1e shows the probability of true positive (p_{TP}), that is, the likelihood of a postsynaptic spike when a presynaptic stimulus is present, for each neuron in the population as a function of V_{PSV}. Clearly, in the absence of any noise each neuron behaves deterministically, that is, the probability of detecting a suprathreshold signals is unity (p_{TP} = 1) whereas the probability of detecting a subthreshold signal is zero (p_{TP} = 0). A histogram of V_{TH} for the neural population is shown in the inset of Figure 1d. As expected, V_{TH} varies across the population owing to variation in the subthreshold slopes and ON currents of the MoS_2 FETs. The population mean and standard deviation of the neural detection threshold was found to be −1.05 V and ∼0.1 V, respectively. Also note that once the presynaptic signal strength falls below the detection threshold of the entire neural population, which was found to be V_{PSV} = −1.25 V, the signal becomes invisible and undetectable.

Adding Synaptic Noise to the Artificial Neural Population. The artificial neurons described above do not accurately mimic biological neurons since neurons are rarely deterministic. In fact, neurons are inherently stochastic. Neural stochasticity, which is a subject of intense research can have numerous biophysical origins.[39] The most dominant and important one for the present study, however, is the synaptic noise, which is attributed to the spontaneous release of neurotransmitter vesicles at the synaptic cleft. The classic manifestation of synaptic noise is random firing of postsynaptic neurons even in the absence of presynaptic input. To introduce stochasticity in our artificial neural population, white Gaussian noise of various standard deviations (σ) was applied to the presynaptic terminal at 100 Hz for a total duration of 5.12 s, and corresponding postsynaptic spikes were recorded for each

https://doi.org/10.1021/acsnano.1c05042
ACS Nano 2021, 15, 16172−16182

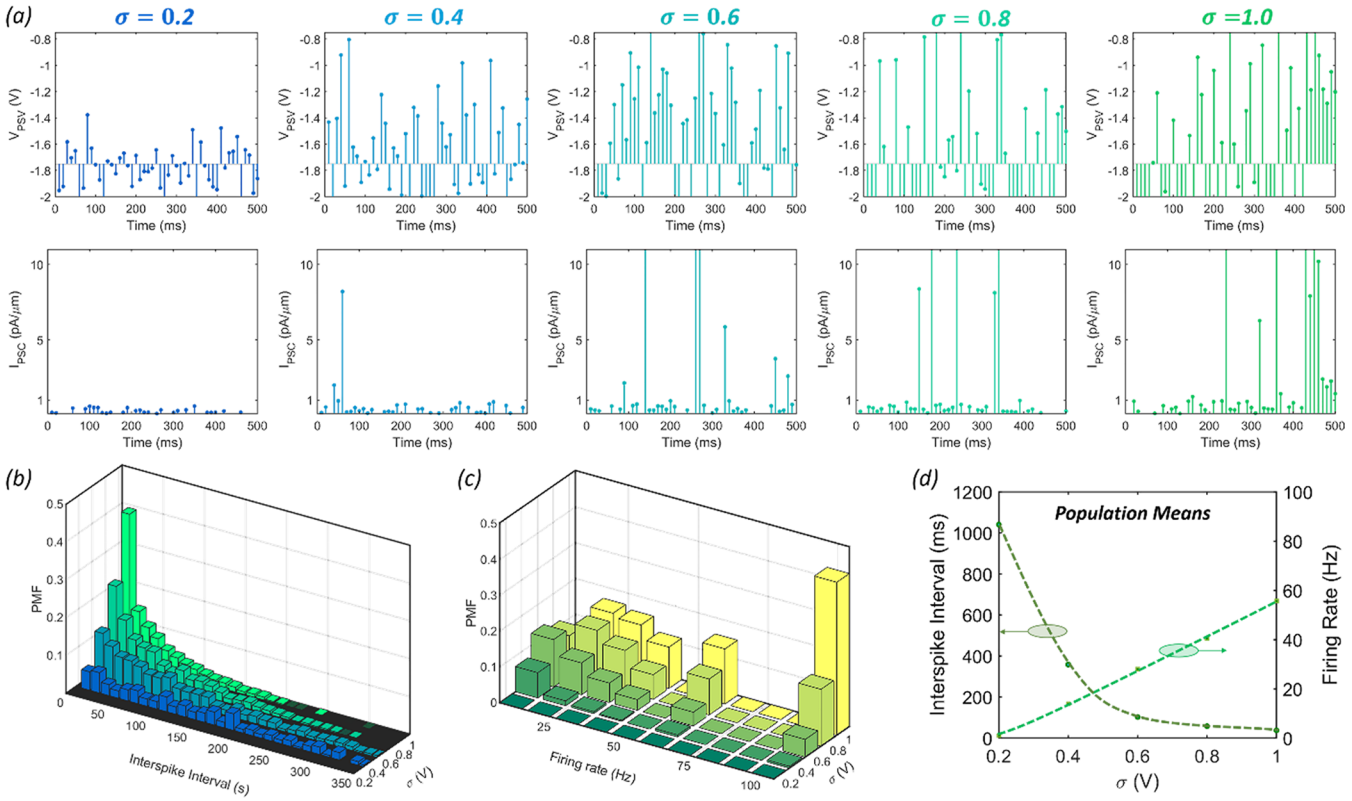

Figure 2. Stochasticity in Neural Population. (a) White Gaussian synaptic noise of various standard deviations (σ) applied to the presynaptic terminal at 100 Hz for a total duration of 5.12 s (upper panel) and corresponding postsynaptic spikes recorded from a representative neuron (lower panel). The mean value for the synaptic noise was set at −1.75 V, which is far below the neural population detection threshold. Random spiking in I_{PSC} increases with increasing σ as the likelihood of crossing the neural detection threshold increases accordingly. Normalized distribution or probability mass function (PMF) for (b) interspike interval and (c) firing rate (i.e., inverse of interspike interval) extracted for the entire neural population, that is, N = 16 neurons. (d) Population mean for interspike interval and firing rate as a function of σ. Lower noise levels lead to sporadic neural spiking manifesting in larger (smaller) population mean in the interspike interval (firing rate), whereas, higher noise levels lead to more frequent neural spiking resulting in smaller (larger) population mean in the interspike interval (firing rate).

neuron of the entire population being recorded. Figure 2a shows the results for a representative neuron. The mean value for the white Gaussian noise was set at −1.75 V, which is far below the neural population detection threshold. Note that the random spiking in postsynaptic current increases with increasing σ as the likelihood of crossing the neural detection threshold increases accordingly. Figure 2b,c, respectively, show the normalized distribution, or probability mass function (PMF), for interspike interval and firing rate (i.e., inverse of interspike interval) for the neural population, that is, N = 16 neurons. Lower noise levels lead to sporadic neural spiking, resulting in larger (smaller) population mean in the interspike interval (firing rate). Conversely, higher noise levels lead to more frequent neural spiking resulting in smaller (larger) population mean in the interspike interval (firing rate) as shown in Figure 2d. Nevertheless, our artificial neurons mimic the stochastic spiking of biological neurons with the added feature that noise level can be programmed independently.

Stochastic Resonance: Benefits of Noise. Noise is an intrinsic feature of the nervous system with diverse roles in neural information processing and transmission. In classical electronic devices and systems, noise is considered to be a nuisance for signal detection. Interestingly, however, noise is not always a problem for neurons and can become a solution for processing critical information pertaining to the survival of the species. SR is a process by which nonlinear threshold-like systems can detect otherwise invisible subthreshold signals in the presence of an optimum amount of noise. Here we exploit SR in our biomimetic neurons. Figure 3a shows a presynaptic subthreshold signal with additive synaptic white Gaussian noise of various standard deviations (σ) and the corresponding postsynaptic spikes from a representative neuron (see Supporting Information 2 for similar results for the entire neural population). Colormaps in Figure 3b−d shows the probability of true positive (p_{TP}), false positive (p_{FP}), and neural detectivity ($D = p_{TP} - p_{FP}$) as a function of σ for N = 16 neurons, respectively. At a low noise level, there is hardly any false firing (low p_{FP}), though the likelihood of detecting the subthreshold presynaptic signal is also restricted due to limited threshold crossing events (low p_{TP}), thus leading to low detectivity. At a high noise level, the subthreshold signal frequently crosses the threshold and invokes postsynaptic spikes (high p_{TP}), but the detectivity still remains low due to excessive false firing (high p_{FP}). However, with an optimum amount of noise, it is possible to achieve maximum detectivity for any individual neuron in the population. Figure 3e shows the population mean for p_{TP}, p_{FP}, and D as a function of σ. Note that the population mean for D exhibits classical SR type behavior.

Figure 3f,g shows normalized PMF for interspike interval and firing frequency as a function of σ for the entire neural population, respectively. Since the subthreshold presynaptic

https://doi.org/10.1021/acsnano.1c05042
ACS Nano 2021, 15, 16172−16182

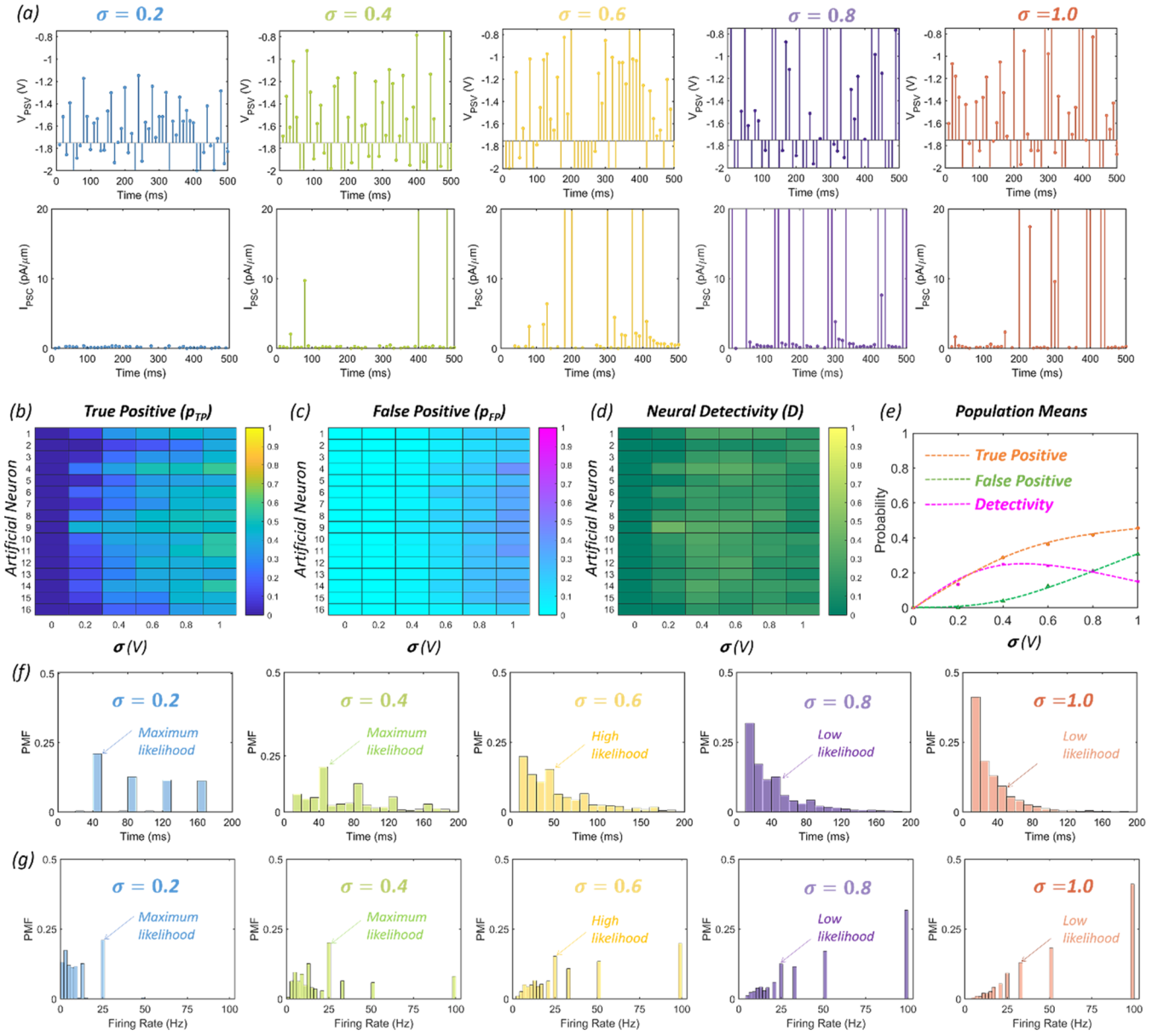

Figure 3. (a) Presynaptic subthreshold signal with additive synaptic white Gaussian noise of various standard deviations, σ, (upper panel) and the corresponding recording of postsynaptic spikes from a representative neuron (lower panel). Colormaps of probability of (b) true positive (p_{TP}), (c) false positive (p_{FP}), and (d) neural detectivity ($D = p_{TP} - p_{FP}$) as a function of σ for $N = 16$ neurons. (e) Corresponding population means. At low noise level, there is hardly any false firing (low p_{FP}), but the likelihood of detecting the subthreshold presynaptic signal is also limited due to limited threshold crossing events (low p_{TP}) leading to low detectivity. At high noise level, the subthreshold signal frequently crosses the threshold invoking postsynaptic spikes (high p_{TP}), but the detectivity still remains low due to excessive false firing (high p_{FP}). However, with optimum amount of noise, it is possible to achieve maximum detectivity for any individual neuron in the population. Note that the population mean for D exhibits classical SR type behavior. Normalized distribution or probability mass function (PMF) for (f) interspike interval and (g) firing frequency as a function of σ for the entire neural population. At optimum synaptic noise, any individual neuron of the neural population can identify the subthreshold presynaptic stimulus, which is presented every 40 ms corresponding to a signal frequency of 25 Hz, with maximum likelihood.

stimulus is presented every 40 ms corresponding to a signal frequency of 25 Hz, it is important that the interspike interval and firing frequency of the postsynaptic neurons reflect such information. This is indeed the case as indicated using the arrows in Figure 3f,g, when compared to random neural spiking in the absence of any stimulus (Figure 2b,c). With optimum noise it is possible to reach maximum likelihood for identifying the signal frequency.

Population Coding: Benefits of Collective Detection. While SR aids in the detection of subthreshold signals, it does not guarantee timely and unambiguous signal detection, which can be critical for the survival of the animals in resource constrained environments. This is because the subthreshold sensory signal may not necessarily cross the detection threshold of a given neuron every time the same stimulus is presented. This is also reflected in the mean detectivity value in Figure 3e, which does not reach unity for any given noise. Similarly, the maximum likelihood for identifying the signal frequency is far from unity (Figure 3g). However, if, instead of studying the activity of neurons in the population individually,

https://doi.org/10.1021/acsnano.1c05042
ACS Nano 2021, 15, 16172−16182

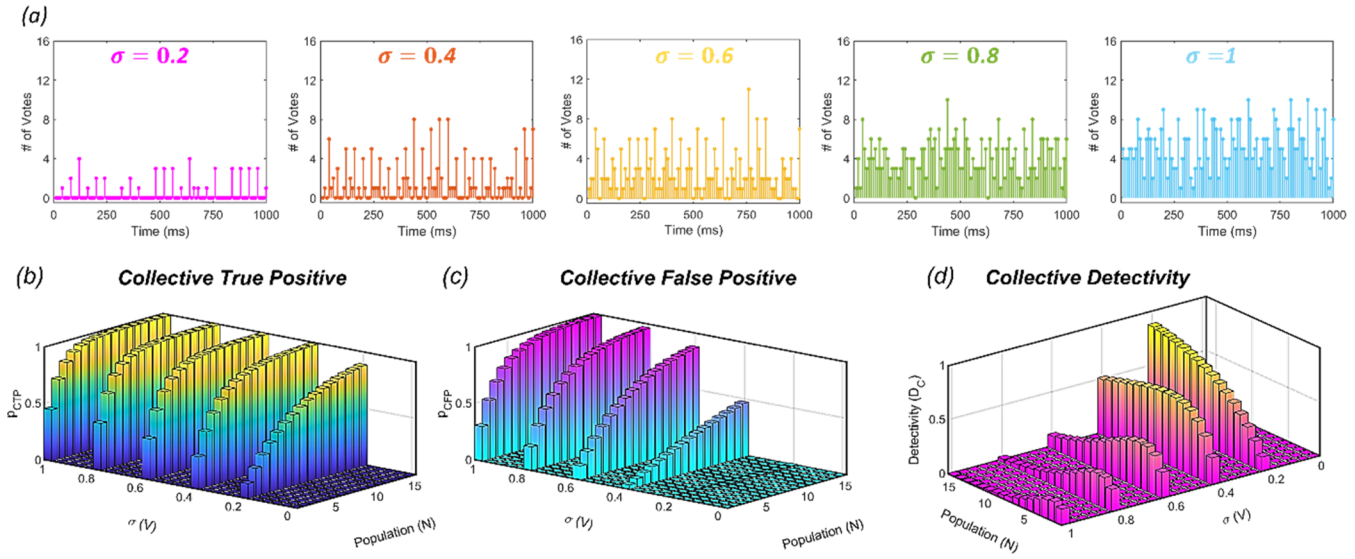

Figure 4. (a) Vote counts, that is, the number of postsynaptic neurons firing in response to the presynaptic subthreshold stimulus with various amount of synaptic white Gaussian noise added to the signal. A true positive is counted if the number of votes is nonzero when the subthreshold presynaptic stimulus is present. Similarly, a false positive is counted even if only one neuron votes in the absence of any presynaptic stimulus. Population mean for the probability of (b) collective true positive (p_{CTP}), (c) collective false positive (p_{CFP}), and (d) collective detectivity (D_C) as a function of σ and the population size, $N = k$, where, $k = 1,2,3\cdots16$, extracted from the corresponding probability distributions shown in Supporting Information 3. Three key features can be observed in D_C. (1) For any finite amount of noise, there is a nonmonotonic trend in D_C as a function of the population size, that is, maximum D_C is achieved for an optimum population size. This can be attributed to the fact that a smaller population is less likely to detect the subthreshold signal, whereas, larger population is more likely to fire falsely in the absence of the signal. (2) For smaller population sizes, classic SR type behavior is seen, that is, there is an optimum noise that allows the population to achieve maximum D_C. (3) For larger population sizes, higher noise is detrimental due to excessive false positive ($p_{CFP} = 1$) despite higher likelihood of detecting a true positive ($p_{CTP} = 1$). Nevertheless, an optimum neural population in the presence of an optimum noise can offer a collective probability for subthreshold signal detection (D_C), which is significantly better than what individual neurons in the same population can achieve.

focus is held on their collective activity, the outcome changes dramatically. Figure 4a shows the vote counts, that is, the number of postsynaptic neurons that fired in response to the presynaptic subthreshold stimulus, in the presence of various amount of synaptic white Gaussian noise. A true positive is counted if one or more neurons out of the entire population generate a postsynaptic spike, that is, the number of votes is nonzero, when the subthreshold presynaptic stimulus is present. Similarly, a false positive is counted even if only one neuron votes by generating a postsynaptic spike in the absence of any presynaptic stimulus. Supporting Information 3 shows the probability distribution of collective true positive (p_{CTP}), false positive (p_{CFP}), and detectivity (D_C) as a function of σ and the population size, $N = k$, where $k = 1,2,3\cdots16$. Figure 4b–d shows the corresponding population means, respectively. Note that all ${}^{N}C_{k}$ combinations for the population were analyzed to derive the results.

There are three key features that can be observed in D_C in Figure 4d. The first is that for any finite amount of noise, there is a nonmonotonic trend in D_C as a function of the population size, that is, maximum D_C is achieved for an optimum population size. This can be attributed to the fact that a smaller population is less likely to detect the subthreshold signal, whereas a larger population is more likely to fire falsely in the absence of the signal. The second is that for smaller population sizes, classic SR type behavior is seen, that is, there is an optimum noise that allows the population to achieve maximum D_C. (3) Finally for larger population sizes, higher noise is detrimental due to excessive false positives ($p_{CFP} = 1$) despite a higher likelihood of detecting a true positive ($p_{CTP} = 1$). Nevertheless, an optimum neural population in the presence of an optimum noise can offer a collective probability for subthreshold signal detection (D_C), which is significantly better than what individual neurons in the same population can achieve. See Supporting Information 4 for the distribution of interspike interval and firing frequency as a function of σ when the entire neural population of $N = 16$ is used for decision making. The likelihood of identifying the signal frequency is high for low noise levels but reduces significantly with increasing noise levels. However, PC improves likelihood of identification more than what can be accomplished through SR using individual neurons for $\sigma = 0.2$ V.

Population Voting: Benefits of Democratic Decision Making. In simple population coding, as described above, even a single neuron can change the decision of the entire neural population regarding the presence or absence of the subthreshold stimulus. It aids in signal detection when the subthreshold signal is present and none other than the "champion" neuron detects the signal. However, it equally hurts when only the "antagonist" neuron fires in the absence of the subthreshold stimulus, increasing the count for false positive. In fact, the poor detectivity of larger neural populations can be attributed to such "antagonist" neural firing. In such cases, decision making based on democratic principles can improve the neural detectivity. Figure 5a,b shows the probability distribution for the number of neurons in the entire population that generate synchronous spikes in response to the presence (true positive) and absence (false positive), respectively, of presynaptic subthreshold signal for different noise standard deviations and for a population size of

https://doi.org/10.1021/acsnano.1c05042
ACS Nano 2021, 15, 16172–16182

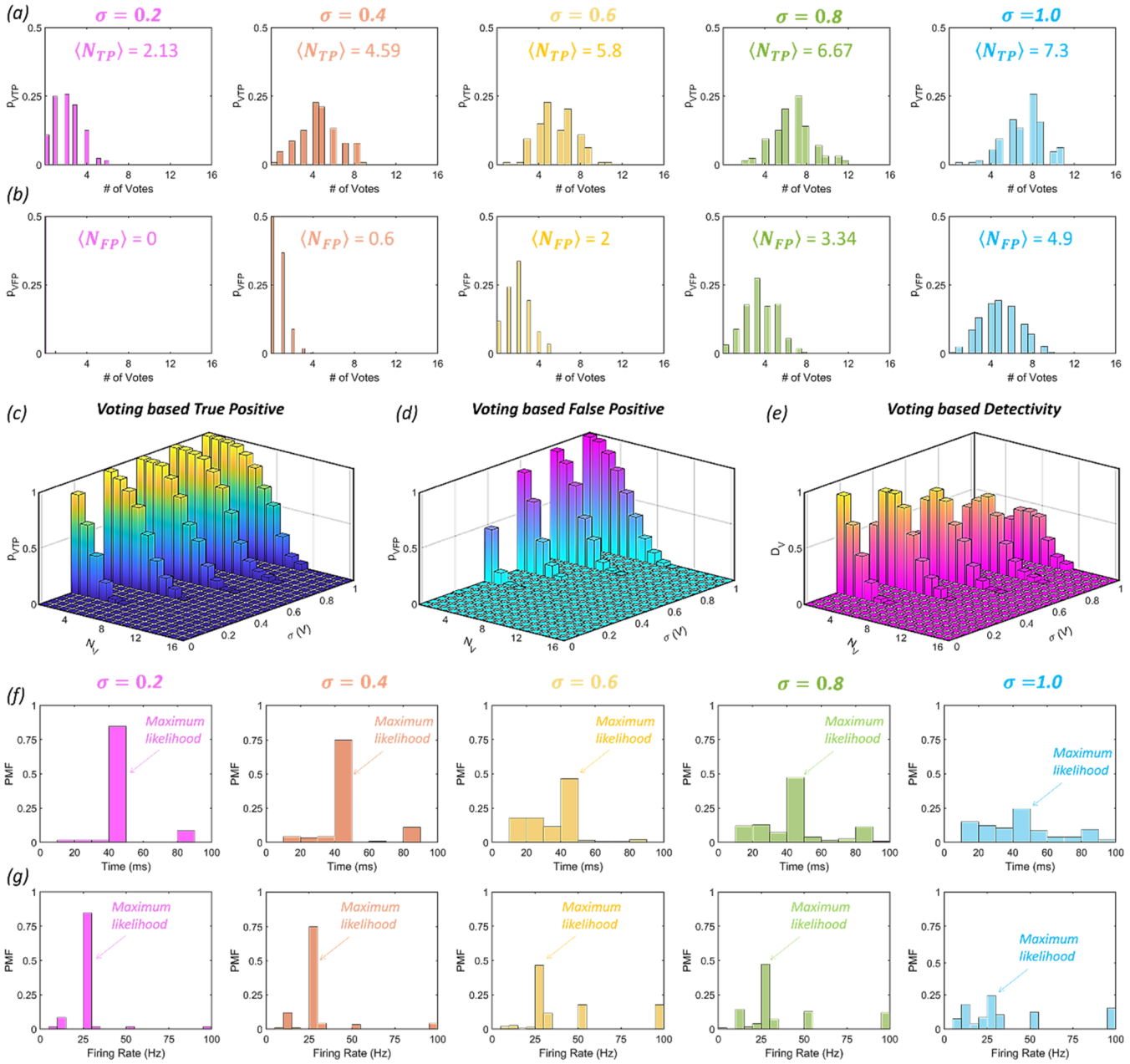

Figure 5. Probability distribution for the number of neurons in the entire population that generate synchronous spikes, that is, the number of votes in response to the (a) presence (true positive) and (b) absence (false positive) of presynaptic subthreshold signal for different noise standard deviations and for a population size of N = 16. Inset shows the expected number of votes. Note that for any noise standard deviation, $\langle N_{TP}\rangle$ is higher than $\langle N_{FP}\rangle$ Probability of voting based (c) true positive (p_{VTP}), (d) false positive (p_{VFP}), and (e) detectivity (D_V) as a function of σ and the minimum number of votes mandated (N_V) for decision making, that is, a true positive or false positive is counted if at least (N_V neurons vote (generate postsynaptic spikes). Note that the detectivity for any given σ reaches its peak value when $N_V = \langle N_{TP}\rangle$. Normalized distribution or probability mass function (PMF) of (g) interspike interval and (h) firing frequency for different σ derived based on population voting. A significant increase in the likelihood of identifying the signal frequency is seen compared to what can be achieved through SR in individual neurons as well as simple population coding highlighting the importance of population voting in the evolutionary success of animals surviving in resource constrained ambience.

N = 16. At low noise levels, the probability of crossing the detection threshold is low and hence only a few neurons fire simultaneously. This makes the expected number of neurons, $\langle N_{TP}\rangle = \sum_{n=1}^{16} np_{VTP}(n)$, to fire synchronously in the presence of the subthreshold presynaptic signal to be low for a low level of noise. The expected number of neurons, $\langle N_{FP}\rangle = \sum_{n=1}^{16} np_{VFP}(n)$, to fire synchronously in the absence of the subthreshold signal is even lower. Similarly, at high noise levels, the probability of crossing the detection threshold is higher and hence more neurons fire synchronously resulting in larger $\langle N_{TP}\rangle$ and $\langle N_{FP}\rangle$. However, for any noise standard deviation, $\langle N_{TP}\rangle$ is higher than $\langle N_{FP}\rangle$ (see Supporting Information 5 for $\langle N_{TP}\rangle$ and $\langle N_{TP}\rangle$ as a function of σ. Figure 5c–e shows the voting-based true positive (p_{VTP}), false positive (p_{VFP}), and detectivity (D_V), respectively, as a function of σ and the minimum number of votes mandated (N_V) for decision making, that is, a true positive or false positive is

https://doi.org/10.1021/acsnano.1c05042
ACS Nano 2021, 15, 16172–16182

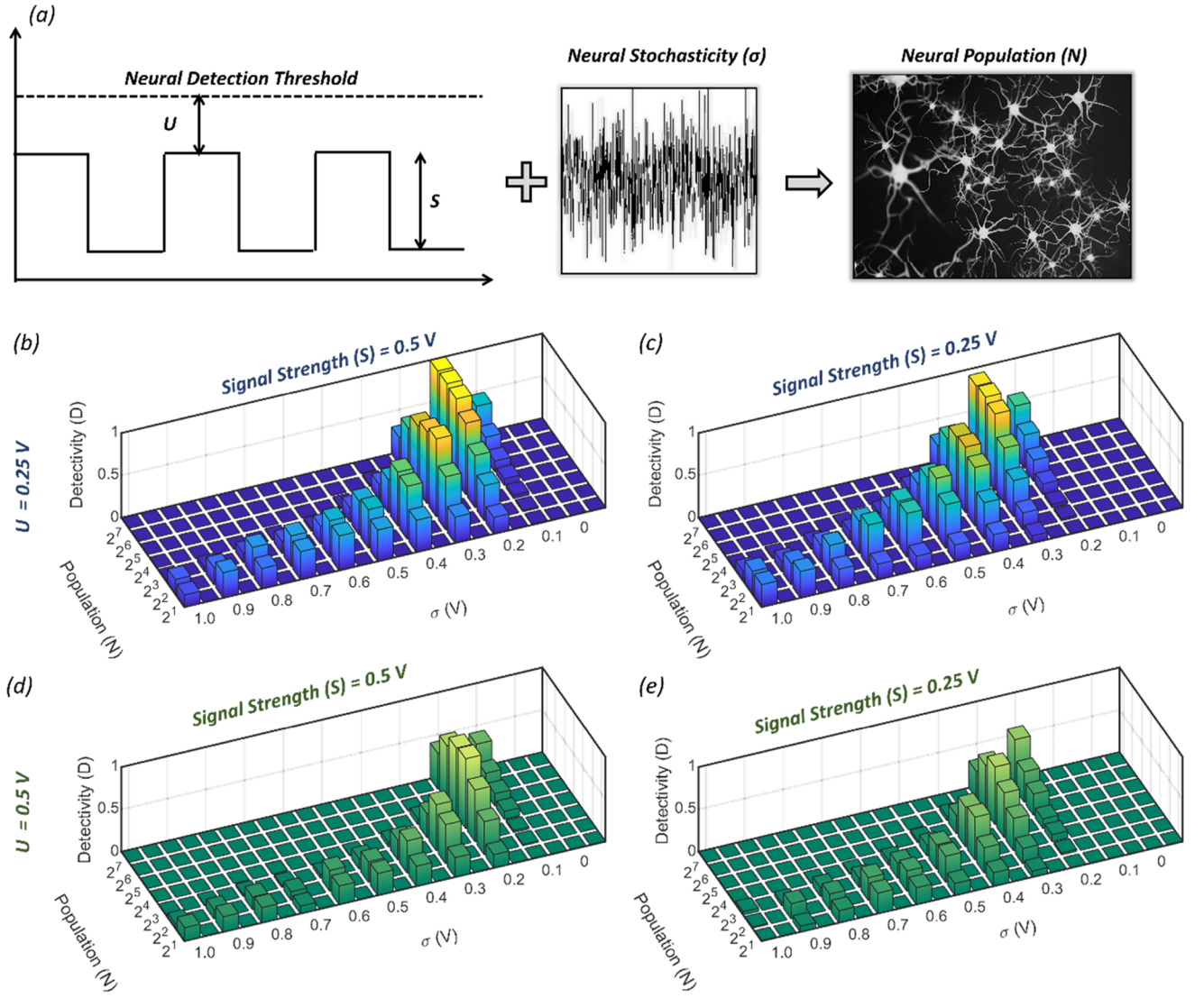

Figure 6. (a) Various factors influencing SR and PC, which include the subthreshold signal strength (S), neural detection threshold (U), neural population strength (N), and neural stochasticity (σ). Simulation results based on Virtual Source (VS) model showing the neural detectivity (D) as a function of N and σ for (b) U = 0.25 V, S = 0.5 V, (c) U = 0.25 V, S = 0.25 V, (d) U = 0.5 V, S = 0.5 V, and (e) U = 0.5 V, S = 0.25 V. In all cases nonmonotonic trends are observed in D as a function of N for any finite σ, and classic SR type behavior is observed in D as a function of σ for any N. Furthermore, for a given S, D diminishes with increasing U and necessitates larger N and higher σ to achieve better detectivity, and for a given U, D diminishes with decreasing S.

counted if at least N_V neurons vote (generate postsynaptic spikes). Note that the detectivity for any given σ reaches its peak value when $N_V = \langle N_{TP} \rangle$. Figure 5g,h shows the normalized PMF for interspike interval and firing frequency for different σ derived on the basis of population voting, respectively. A significant increase in the likelihood of identifying the signal frequency is seen compared to what can be achieved through SR in individual neurons as well as simple population coding highlighting the importance of population voting in the evolutionary success of animals surviving in resource-constrained environments. Interestingly, the energy consumption by the biomimetic, stochastic, and artificial neural population based on the monolayer MoS_2 FET array was found to be as frugal as hundreds of femto Joules per spike per neuron (see Supporting Information 6).

Neural Interplay between Stochastic Resonance and Population Coding. In order to extend the conclusion drawn from our experimental findings, physics-based numerical simulations were used to elucidate the interplay between SR and PC, as shown in Figure 6. We have used the Virtual Source (VS) model to capture the transfer function of our artificial neurons based on monolayer MoS_2 FET.[40−42] In the VS model, both the subthreshold and above-threshold behavior is captured through a single semiempirical and phenomenological relationship (see Supporting Information 7 for the description of the VS model). Figure 6a−e shows the various factors and their interdependence influencing SR and PC, which include the subthreshold signal strength (S), neural detection threshold (U), neural population strength (N), and neural stochasticity (σ). The key features observed in the experimental data in Figure 4d are also seen in each of the four simulated case studies presented here. These are the nonmonotonic trend in D as a function of the population size for any finite amount of noise, and classic SR type behavior in D as a function of noise standard deviation (σ) for any population size. In addition, we observe that for a given S, D

https://doi.org/10.1021/acsnano.1c05042
ACS Nano 2021, 15, 16172−16182

diminishes with increasing U and necessitates larger N and higher σ to achieve better detectivity. This is anticipated as a smaller number of threshold crossing events occur for a given σ when the signal is far away from U. Similarly, as the signal becomes weaker (smaller S), the D also diminishes for a given neural detection threshold. However, in this case, lower noise and larger population achieves better detectivity as higher noise can lead to excessive false firing. Nevertheless, by exploiting the synergy between SR and PC, a biomimetic and artificial nervous system can accomplish accurate and timely detection of subthreshold signals, which can benefit edge sensors in the IoT era.

CONCLUSION

In conclusion, we have used a biomimetic, stochastic, and artificial neural population based on monolayer MoS_2 FET array to demonstrate the benefits of stochastic resonance, population coding, and population voting for detecting otherwise invisible subthreshold signals at ultralow energy expenditure. Our study not only offers insight for the next generation of bioinspired sensors for deployment in resource-constrained locations but also demonstrates how such biomimetic nanoscale devices can be used to advance the fundamental understanding of intricate neural processes in sensory neurobiology.

METHODS

Film Growth. Monolayer MoS_2 obtained from the Two Dimensional Crystal Consortium (2DCC) at Penn State University was deposited on epi-ready 2″ c-sapphire substrate by metalorganic chemical vapor deposition (MOCVD). An inductively heated graphite susceptor equipped with wafer rotation in a cold-wall horizontal reactor was used to achieve uniform monolayer deposition as previously described.[43] Molybdenum hexacarbonyl ($Mo(CO)_6$) and hydrogen sulfide (H_2S) were used as precursors. $Mo(CO)_6$ maintained at 10 °C and 950 Torr in a stainless steel bubbler was used to deliver 0.036 sccm of the metal precursor for the growth, while 400 sccm of H_2S was used for the process. MoS_2 deposition was carried out at 1000 °C and 50 Torr in H_2 ambient, where monolayer growth was achieved in 18 min. The substrate was first heated to 1000 °C in H_2 and maintained for 10 min before the growth was initiated. After growth, the substrate was cooled in H_2S to 300 °C to inhibit decomposition of the MoS_2 films.

Film Transfer. After the growth of monolayer MoS_2 on the sapphire substrate, the film was transferred onto the FET gate dielectric substrate using a wet transfer technique. Polymethylmethacrylate (A3 PMMA) resist was spun onto the growth substrate at 400 rpm for 45 s, encapsulating the MoS_2, and allowed to sit overnight. The substrate was then immersed in a 1 M NaOH solution kept at 90 °C. Capillary action at the PMMA/substrate interface allowed for intercalation of the NaOH solution, separating the hydrophobic PMMA/MoS_2 from the hydrophilic sapphire substrate and allowing the film to float to the surface of the solution. A clean glass slide was used to transfer the PMMA/MoS_2 stack to three successive deionized water baths for cleaning, before finally fishing out the film with the target alumina/Pt/TiN/p^{++} Si substrate.[44]

Fabrication of Monolayer MoS_2 FET. Back-gated MoS_2 field effect transistors (FETs) were fabricated on 50 nm alumina (Al_2O_3), which served as the back-gate oxide, and a stack of Pt/TiN/p^{++} Si, which served as the back-gate electrode. First, MOCVD-grown MoS_2 was transferred onto the alumina substrate as previously described. The sample was then spin-coated with A6 PMMA and patterned via electron-beam (e-beam) lithography to specify the channels. A 30 s sulfur hexafluoride (SF_6) etch at 5 °C was then used to define the channels. Following the etch step, the sample was sequentially rinsed in acetone for 30 min and isopropyl alcohol (IPA) for 15 min to remove the PMMA and clean off any residue. To define the source and drain contacts, the sample was then spin-coated with methyl methacrylate (MMA) and A3 PMMA, and e-beam lithography was again used for patterning. 40 nm of nickel (Ni) and 30 nm of gold (Au) were deposited using e-beam evaporation to serve as the contact metal, with the Ni-layer serving to improve adhesion. Finally, lift-off of the evaporated metal was performed by immersing the sample in acetone for 30 min, with a subsequent IPA bath for cleaning.

Electrical Characterization. Electrical characterization of the fabricated devices was performed on a Lake Shore CRX-VF probe station under atmospheric conditions using a Keysight B1500A parameter analyzer.

ASSOCIATED CONTENT

Supporting Information

The Supporting Information is available free of charge at https://pubs.acs.org/doi/10.1021/acsnano.1c05042.

Material characterization of metal−organic chemical vapor deposition (MOCVD) grown MoS_2, recording of the postsynaptic currents of the entire neural population (N = 16) in response to presynaptic voltages, probability distribution of true positive, false positive and detectivity of the neural population based on population coding, distribution of interspike interval and firing frequency for different standard deviations of noise (σ), expected number of votes as a function of σ for N = 16, the average energy expenditure (E) per spike per neuron as a function of σ, and the description of virtual source model and corresponding simulated and experimental transfer characteristics (PDF)

AUTHOR INFORMATION

Corresponding Author

Saptarshi Das − *Department of Engineering Science and Mechanics, Department of Materials Science and Engineering, and Materials Research Institute, Pennsylvania State University, University Park, Pennsylvania 16802, United States*; orcid.org/0000-0002-0188-945X; Email: sud70@psu.edu, das.sapt@gmail.com

Author

Akhil Dodda − *Department of Engineering Science and Mechanics, Pennsylvania State University, University Park, Pennsylvania 16802, United States*

Complete contact information is available at: https://pubs.acs.org/10.1021/acsnano.1c05042

Author Contributions

S.D. conceived the idea. A.D. and S.D. designed and performed the experiments, analyzed the data, discussed the results, and agreed on their implications. All authors contributed to the preparation of the manuscript.

Notes

The authors declare no competing financial interest.

ACKNOWLEDGMENTS

The work was supported by the Army Research Office (ARO) through Contract Number W911NF1920338 and the National Science Foundation (NSF) through CAREER Award under Grant Number ECCS-2042154. We also acknowledge Mr. Amritanand Sebastian for help with device fabrication. Authors also acknowledge the materials support from the National Science Foundation (NSF) through the Pennsylvania State

University 2D Crystal Consortium—Materials Innovation Platform (2DCCMIP) under NSF cooperative agreement DMR-1539916.

REFERENCES

(1) Douglass, J. K.; Wilkens, L.; Pantazelou, E.; Moss, F. Noise Enhancement of Information Transfer in Crayfish Mechanoreceptors by Stochastic Resonance. *Nature* **1993**, *365*, 337.
(2) Russell, D. F.; Wilkens, L. A.; Moss, F. Use of Behavioural Stochastic Resonance by Paddlefish for Feeding. *Nature* **1999**, *402*, 291.
(3) Levin, J. E.; Miller, J. P. Broadband Neural Encoding in the Cricket Cereal Sensory System Enhanced by Stochastic Resonance. *Nature* **1996**, *380*, 165.
(4) Wiesenfeld, K.; Moss, F. Stochastic Resonance and the Benefits of Noise: From Ice Ages to Crayfish and SQUIDs. *Nature* **1995**, *373*, 33.
(5) Schmitz, H.; Bousack, H. Modelling a Historic Oil-Tank Fire Allows an Estimation of the Sensitivity of the Infrared Receptors in Pyrophilous Melanophila Beetles. *PLoS One* **2012**, *7*, e37627.
(6) Lindner, B.; Schimansky-Geier, L. Transmission of Noise Coded versus Additive Signals through a Neuronal Ensemble. *Phys. Rev. Lett.* **2001**, *86*, 2934−2937.
(7) Dean, I.; Harper, N. S.; McAlpine, D. Neural Population Coding of Sound Level Adapts to Stimulus Statistics. *Nat. Neurosci.* **2005**, *8*, 1684−1689.
(8) Georgopoulos, A. P.; Schwartz, A. B.; Kettner, R. E. Neuronal Population Coding of Movement Direction. *Science* **1986**, *233*, 1416−1419.
(9) Averbeck, B. B.; Latham, P. E.; Pouget, A. Neural Correlations, Population Coding and Computation. *Nat. Rev. Neurosci.* **2006**, *7*, 358−366.
(10) Pasupathy, A.; Connor, C. E. Population Coding of Shape in Area V4. *Nat. Neurosci.* **2002**, *5*, 1332−1338.
(11) Petersen, R. S.; Panzeri, S.; Diamond, M. E. Population Coding of Stimulus Location in Rat Somatosensory Cortex. *Neuron* **2001**, *32*, 503−514.
(12) Georgopoulos, A. P.; Kettner, R. E.; Schwartz, A. B. Primate Motor Cortex and Free Arm Movements to Visual Targets in Three-Dimensional Space. II. Coding of the Direction of Movement by a Neuronal Population. *J. Neurosci.* **1988**, *8*, 2928−2937.
(13) Georgopoulos, A. P.; Lurito, J. T.; Petrides, M.; Schwartz, A. B.; Massey, J. T. Mental Rotation of the Neuronal Population Vector. *Science* **1989**, *243*, 234−236.
(14) Stacey, W. C.; Durand, D. M. Synaptic Noise Improves Detection of Subthreshold Signals in Hippocampal CA1 Neurons. *J. Neurophysiol.* **2001**, *86*, 1104−1112.
(15) Mantegna, R.; Spagnolo, B. Stochastic Resonance in a Tunnel Diode. *Phys. Rev. E: Stat. Phys., Plasmas, Fluids, Relat. Interdiscip. Top.* **1994**, *49*, R1792.
(16) Dodda, A.; Oberoi, A.; Sebastian, A.; Choudhury, T. H.; Redwing, J. M.; Das, S. Stochastic Resonance in MoS2 Photodetector. *Nat. Commun.* **2020**, *11*, 4406.
(17) Kawahara, T.; Yamaguchi, S.; Maehashi, K.; Ohno, Y.; Matsumoto, K.; Kawai, T. Robust Noise Modulation of Nonlinearity in Carbon Nanotube Field-Effect Transistors. *Jpn. J. Appl. Phys.* **2010**, *49*, 02BD11.
(18) Hakamata, Y.; Ohno, Y.; Maehashi, K.; Inoue, K.; Matsumoto, K. Robust Noise Characteristics in Carbon Nanotube Transistors Based on Stochastic Resonance and Their Summing Networks. *Jpn. J. Appl. Phys.* **2011**, *50*, 06GE03.
(19) Nishiguchi, K.; Fujiwara, A. Detecting Signals Buried in Noise via Nanowire Transistors Using Stochastic Resonance. *Appl. Phys. Lett.* **2012**, *101*, 193108.
(20) Suzuki, Y.; Asakawa, N. Robust Thresholdlike Effect of Internal Noise on Stochastic Resonance in an Organic Field-Effect Transistor. *Phys. Rev. E: Stat. Phys., Plasmas, Fluids, Relat. Interdiscip. Top.* **2018**, *97*, 012217.
(21) Butler, S. Z.; Hollen, S. M.; Cao, L.; Cui, Y.; Gupta, J. A.; Gutierrez, H. R.; Heinz, T. F.; Hong, S. S.; Huang, J.; Ismach, A. F.; Johnston-Halperin, E.; Kuno, m.; Plashnitsa, V. V.; Robinson, R. D.; Ruoff, R. S.; Salahuddin, S.; Shan, J.; Shi, L.; Spencer, M. G.; Terrones, M.; et al. Progress, Challenges, and Opportunities in Two-Dimensional Materials beyond Graphene. *ACS Nano* **2013**, *7*, 2898−2926.
(22) Bhimanapati, G. R.; Lin, Z.; Meunier, V.; Jung, y.; Cha, J.; Das, S.; Xiao, D.; Son, Y.; Strano, M. S.; Cooper, V. R.; Liang, L.; Louie, S. G.; Ringe, E.; Zhou, W.; Kim, S. S.; Naik, R. R.; Sumpter, B. G.; Terrones, H.; Xia, F.; Wang, Y.; et al. Recent Advances in Two-Dimensional Materials beyond Graphene. *ACS Nano* **2015**, *9*, 11509−11539.
(23) Das, S.; Robinson, J. A.; Dubey, M.; Terrones, H.; Terrones, M. Beyond Graphene: Progress in Novel Two-Dimensional Materials and van der Waals Solids. *Annu. Rev. Mater. Res.* **2015**, *45*, 1−27.
(24) Schulman, D. S.; Arnold, A. J.; Das, S. Contact Engineering for 2D Materials and Devices. *Chem. Soc. Rev.* **2018**, *47*, 3037−3058.
(25) Sebastian, A.; Pendurthi, R.; Choudhury, T. H.; Redwing, J. M.; Das, S. Benchmarking Monolayer MoS2 and WS2 Field-Effect Transistors. *Nat. Commun.* **2021**, *12*, 693.
(26) Daus, A.; Vaziri, S.; Chen, V.; Köroğlu, C.; Grady, R. W.; Bailey, C. S.; Lee, H. R.; Schauble, K.; Brenner, K.; Pop, E. High-performance Flexible Nanoscale Transistors Based on Transition Metal Dichalcogenides. *Nat. Electron.* **2021**, 4495.
(27) Li, H.; Li, Y.; Aljarb, A.; Shi, Y.; Li, L. J. Epitaxial Growth of Two-Dimensional Layered Transition Metal Dichalcogenides: Growth Mechanism, Controllability, and Scalability. *Chem. Rev.* **2018**, *118* (13), 6134−6150.
(28) Lanza, M.; Smets, Q.; Huyghebaert, C.; Li, L. J. Yield, Variability, Reliability, and Stability of Two-Dimensional Materials Based Solid-State Electronic Devices. *Nat. Commun.* **2020**, *11*, 5689.
(29) Lee, G.-H.; Cui, X.; Kim, Y. D.; Arefe, G.; Zhang, X.; lee, C.; Ye, F.; Watanabe, K.; Taniguchi, T.; Kim, P.; Hone, J. Highly Stable, Dual-Gated MoS2 Transistors Encapsulated by Hexagonal Boron Nitride with Gate-Controllable Contact, Resistance, and Threshold Voltage. *ACS Nano* **2015**, *9*, 7019−7026.
(30) Wali, A.; Kundu, S.; Arnold, A. J.; Zhao, G.; Basu, K.; Das, S. Satisfiability Attack-Resistant Camouflaged Two-Dimensional Heterostructure Devices. *ACS Nano* **2021**, *15*, 3453−3467.
(31) Subbulakshmi Radhakrishnan, S.; Sebastian, A.; Oberoi, A.; Das, S.; Das, S. A Biomimetic Neural Encoder for Spiking Neural Network. *Nat. Commun.* **2021**, *12*, 2143.
(32) Nasr, J. R.; Simonson, N.; Oberoi, A.; Horn, M. W.; Robinson, J. A.; Das, S. Low-Power and Ultra-Thin MoS2 Photodetectors on Glass. *ACS Nano* **2020**, *14*, 15440−15449.
(33) Jayachandran, D.; Oberoi, A.; Sebastian, A.; Choudhury, T. M.; Shankar, B.; Redwing, J. M.; Das, S. A Low-Power Biomimetic Collision Detector Based on an In-Memory Molybdenum Disulfide Photodetector. *Nature Electronics* **2020**, *3*, 646−655.
(34) Arnold, A. J.; Schulman, D. S.; Das, S. Thickness Trends of Electron and Hole Conduction and Contact Carrier Injection in Surface Charge Transfer Doped 2D Field Effect Transistors. *ACS Nano* **2020**, *14*, 13557−13568.
(35) Arnold, A. J.; Razavieh, A.; Nasr, J. R.; Schulman, D. S.; Eichfeld, C. M.; Das, S. Mimicking Neurotransmitter Release in Chemical Synapses via Hysteresis Engineering in MoS2 Transistors. *ACS Nano* **2017**, *11*, 3110−3118.
(36) Das, S. Two Dimensional Electrostrictive Field Effect Transistor (2D-EFET): A sub-60mV/Decade Steep Slope Device with High ON Current. *Sci. Rep.* **2016**, *6*, 34811.
(37) Zhang, F.; Erb, C.; Runkle, L.; Zhang, X.; Alem, N. Etchant-Free Transfer of 2D Nanostructures. *Nanotechnology* **2018**, *29*, 025602.
(38) Das, S.; Chen, H. Y.; Penumatcha, A. V.; Appenzeller, J. High Performance Multilayer MoS2 Transistors with Scandium Contacts. *Nano Lett.* **2013**, *13*, 100−105.
(39) Faisal, A. A.; Selen, L. P. J.; Wolpert, D. M. Noise in the Nervous System. *Nat. Rev. Neurosci.* **2008**, *9*, 292−303.

https://doi.org/10.1021/acsnano.1c05042
ACS Nano 2021, 15, 16172−16182

(40) Lundstrom, M. S.; Antoniadis, D. A. Compact Models and the Physics of Nanoscale FETs. *IEEE Trans. Electron Devices* **2014**, *61*, 225−233.
(41) Sebastian, A.; Pannone, A.; Radhakrishnan, S. S.; Das, S. Gaussian Synapses for Probabilistic Neural Networks. *Nat. Commun.* **2019**, *10*, 4199.
(42) Das, S.; Dodda, A.; Das, S. A Biomimetic 2D Transistor for Audiomorphic Computing. *Nat. Commun.* **2019**, *10*, 3450.
(43) Xuan, Y.; Jain, A.; Zafar, S.; Lotfi, R.; Nayir, N.; Wang, Y.; Choudhury, T. H.; Wright, S.; Fereca, J.; Rosenbaum, L.; Redwing, J. M.; Crespi, V.; Van Duin, A. C. T. Multi-Scale Modeling of Gas-Phase Reactions in Metal-Organic Chemical Vapor Deposition Growth of WSe2. *J. Cryst. Growth* **2019**, *527*, 527.
(44) Sebastian, A.; Zhang, F.; Dodda, A.; May-Rawdling, D.; Liu, H.; Zhang, T.; Terrones, M.; Das, S. Electrochemical Polishing of Two-Dimensional Materials. *ACS Nano* **2019**, *13*, 78−86.

https://doi.org/10.1021/acsnano.1c05042
ACS Nano 2021, 15, 16172−16182